



# About 300 days Optical Quasi-periodic Oscillations in the Long-term Light Curves of the Blazar PKS 2155-304

Qi Zheng, Xue-Guang Zhang, and Qi-Rong Yuan

School of Physics and Technology, Nanjing Normal University, Nanjing 210023, China; [211002011@njnu.edu.cn](mailto:211002011@njnu.edu.cn), [xgzhang@njnu.edu.cn](mailto:xgzhang@njnu.edu.cn), [yuanqirong@njnu.edu.cn](mailto:yuanqirong@njnu.edu.cn)  
Received 2022 March 14; revised 2022 June 17; accepted 2022 June 21; published 2022 July 22

## Abstract

Based on the long-term light curves collected from the Catalina Sky Survey (CSS) (from 2005 to 2013) and the All-Sky Automated Survey for Supernovae (ASAS-SN) (from 2014 to 2018), optical quasi-periodic oscillations (QPOs) about 300 days can be well determined in the well-known blazar PKS 2155-304 through four different methods: the generalized Lomb-Scargle periodogram (GLSP) method, the weighted wavelet Z-transform technique, the epoch-folded method and the redfit method. The GLSP determined significance level for the periodicity is higher than 99.9999% based on a false alarm probability. The redfit provided confidence level for the periodicity is higher than 99% in the ASAS-SN light curve, after considering the effects of red noise. Based on continuous autoregressive process created artificial light curves, the probability of detecting fake QPOs is lower than 0.8%. The determined optical periodicity of 300 days from the CSS and ASAS-SN light curves is well consistent with the reported optical periodicity in the literature. Moreover, three possible models are discussed to explain the optical QPOs in PKS 2155-304: the relativistic frame-dragging effect, the binary black hole model and the jet precession model.

*Key words:* (galaxies:) BL Lacertae objects: individual (PKS 2155-304) – galaxies: active – (galaxies:) quasars: supermassive black holes

## 1. Introduction

PKS 2155-304 ( $z = 0.116$ ) (Aharonian et al. 2009) is one of the best known blazars and one of the brightest objects from the UV to TeV energies in the southern sky (Carini & Miller 1992; Foschini et al. 2007). With the Parkes survey, PKS 2155-304 has been observed in the radio band (Shimmins & Bolton 1974). Using HEAO-1, Schwartz et al. (1979) completed its first X-ray observations. Due to its strong and variable X-ray emissions, it was classified as a BL Lac object (Zhang et al. 2021). PKS 2155-304 was first identified as a TeV blazar by the detection of VHE gamma-rays by the Durham MK 6 telescopes (Chadwick et al. 1999), and then was confirmed by the H.E.S.S. (Aharonian et al. 2005). PKS 2155-304 has been observed on diverse timescales over a wide range of frequencies from radio to VHE  $\gamma$ -rays, and has shown rapid and strong variability (Miller & McAlister 1983; Fan & Lin 2000). Generally, blazar variability timescale ( $t_{\text{var}}$ ) is divided into three classes (Gupta et al. 2004; Agarwal et al. 2019): microvariability (intra-night variability or intra-day variability, IDV;  $t_{\text{var}} \sim$  less than a day) (Wagner & Witzel 1995), short-term variability (STV;  $t_{\text{var}} \sim$  from days to few months) and long-term variability (LTV;  $t_{\text{var}} \sim$  from months to several years) (Pandey et al. 2020). Through AGN variability, we can obtain information with respect to their nature. It is important for quasar modeling (Fan et al. 1998).

Optical variability of PKS 2155-304 has been studied for many years. PKS 2155-304 has obvious IDV (Paltani et al. 1997; Tommasi et al. 2001; Dominici et al. 2006), STV (Carini & Miller 1992; Pesce et al. 1997) and LTV (Kastendieck et al. 2011) in the optical band, but it also can stay in a completely stable state for one week (Heidt et al. 1997). In addition, the optical variability is related to X-ray (Dominici et al. 2004) and NIR bands (Li et al. 2018). The main focus of this paper is long-term variability in the optical V-band in PKS 2155-304.

The quasi-periodic oscillations (QPOs) in optical band have been found in PKS 2155-304. In the V-band, with data from 1970 onwards, Fan & Lin (2000) reported QPOs of  $T \sim 4.2$  yr and  $T \sim 7.0$  yr, and also put forward a possibility of a periodicity of less than 4 yr, but they could not confirm this periodicity because of the lack of data. In an available historical archival data set (data from 25 different astronomical groups) in the R-band collected for 35 yr (covering 1979–2013), evidence of QPOs with a periodicity of 317 days was reported in Zhang et al. (2014). Rieger & Volpe (2010) discussed that the long-term QPOs in PKS 2155-304 might indicate a binary black hole (BBH) model, leading to a signal of periodicity when the secondary BH crosses the disk of the primary BH, similar as the QPOs in OJ 287 (Valtonen et al. 2008; Hayasaki et al. 2013; Britzen et al. 2020). In addition, with the *VRIJHK* photometry, Sandrinelli et al. (2014) reported QPOs of  $T \sim 315$  days by using data from the Rapid Eye Mounting Telescope

during 2005–2012, which is well consistent with the report by Zhang et al. (2014). What is more, the overlap of time interval between two works makes the periodicity more robust. A few years later, using the extensive HIPPO data taken from 2009 July 25 to 27, Pekeur et al. (2016) claimed QPOs of  $T \sim 13$  minutes and  $T \sim 30$  minutes, which is the first evidence of QPOs in the polarization of AGN, and discussed that such fast variations in the optical polarization might generate from an emission region, which is comparable in size to radius of gravity of the central engine, in Doppler boosted jet. Sandrinelli et al. (2018) derived data from the Rapid Eye Mounting Telescope photometry, SMARTS, the Tuorla Blazar Monitoring Program, and combined with data from the Steward Observatory Fermi Blazar Observational Program, ROTSEIII, the All Sky Automated Survey robotic telescopes and archival data collected by Kastendieck et al. (2011), and found a periodicity of  $315 \pm 25$  days in the  $R$ -band, which can be caused by relativistic jet instabilities (Pandey et al. 2020; Kalita et al. 2021) or chance fluctuation (Hong et al. 2018; Smith et al. 2018). Chevalier et al. (2019) reported that a 700 day-long periodicity is found in the optical band, as well as in high energy ( $100 \text{ MeV} < E < 300 \text{ GeV}$ ) with the combination of SMARTS, RXTE, Swift/XRT, XMM-Newton, Fermi and H.E. S.S. data, which can be explained by a time-dependent synchrotron-self Compton (SSC) (Abdo et al. 2010; Arbet-Engels et al. 2021; Joshi & Razaque 2021) model, except for optical band. In this paper, further evidence of optical QPOs will be given in PKS 2155-304 through long-term variability from the Catalina Sky Survey (CSS) Data Release 2 (Drake et al. 2009) and All-Sky Automated Survey for Supernovae (ASAS-SN) (Shappee et al. 2014; Kochanek et al. 2017).

In other bands, signals of QPOs have also been detected and reported in PKS 2155-304. Urry et al. (1993) reported a  $\sim 0.7$  day QPOs in the ultraviolet from data obtained by the IUE satellite throughout 1991 November on a daily basis, and suggested that the flares may cause from disturbances propagating along magnetic field in a jet. Unfortunately, with more data achieved during the whole month of 1991 November, Edelson et al. (1995) could not recover the periodicity above with more rigorous analysis. Based on the XMM-Newton EPIC/pn detector observation of 24 data sets, Lachowicz et al. (2009) obtained a periodicity of  $T \sim 4.6$  h on 2006 May 1 in the 0.3–10 keV. Gaur et al. (2010) claimed that another light curve, rather than the upper one, from XMM-Newton/EPIC displays a weak and broad QPO with a periodicity of  $5.5 \pm 1.3$  ks. Sandrinelli et al. (2014) considered the Fermi light curve (from 2008 August 6 to 2014 June 9), and pointed out a periodicity peak at  $T \sim 630$ – $640$  days, which is twice as many as optical and NIR period. Zhang et al. (2017) found a  $1.74 \pm 0.13$  year-long  $\gamma$ -ray QPOs in Fermi LAT Pass 8 data with the data from August 2008 to October 2016, probably associated with relativistic jet instability or the process feeding the jet. Moreover, a jets-in-jet model was

purposed as a plausible reason to explain the TeV flares. There are blobs that move relativistically in the jet, which lead to fast-evolving flares (Giannios et al. 2009). Rapid TeV variability can be well explained using a standard SSC approach while taking into account the particle evolution and the external light-crossing time effects (Katarzyński et al. 2008). Prokhorov & Moraghan (2017) provided evidence of a 644 day-long periodicity in  $\gamma$ -ray band from Fermi-LAT (3FGL). The result corresponds to 1.7 yr proposed by Peñil et al. (2020) with same data. Bhatta & Dhital (2020) reported a periodicity of  $\sim 610$  days from 3FGL. Tarnopolski et al. (2020) analyzed data from the LAT 8 yr Source Catalog, spanning from 2008 August 4 to 2019 April 19, and found a periodicity of  $612 \pm 42$  days in  $\gamma$ -ray band, confirmed by Żywucka et al. (2021). According to the long timescale, Żywucka et al. (2021) considered that the variability originates in accretion disk.

This paper is organized as follows. In Section 2, the acquisition of the magnitude measurements, and methods to determine the optical QPOs are presented. Our discussions on the optical QPOs with a periodicity about 300 days are given in Section 3. Final summaries and conclusions are shown in Section 4. Throughout this paper, we have adopted the cosmological parameters of  $H_0 = 70 \text{ km} \cdot \text{s}^{-1} \text{Mpc}^{-1}$ ,  $\Omega_\Lambda = 0.7$  and  $\Omega_m = 0.3$ .

## 2. Main Results

We collected optical-band photometric data of PKS 2155-304 from the CSS (Drake et al. 2009) and from the ASAS-SN (Shappee et al. 2014; Kochanek et al. 2017), with CSS light curve from 2005 August 15 to 2013 July 6 (MJD from 53 597.542 to 56 479.608), with the ASAS-SN light curve from 2014 May 15 to 2018 September 14 (HJD from 2 456 792.777 to 2 458 375.657), shown in Figure 1. CSS utilizes three telescopes, 1.5 m telescope with the field of view  $5.0 \text{ deg}^2$ , 1.0 m telescope with the field of view  $0.3 \text{ deg}^2$ , 0.7 m telescope with the field of view  $19.4 \text{ deg}^2$ , owned and managed by Steward Observatory of the University of Arizona. The CSS is a part of the Catalina Surveys. The CSS project is mainly used for searching rapidly moving Near Earth Objects (NEOs) and makes efforts to catalog at least 90 percent of the estimated population of NEOs larger than 140 m, some of which may pose an impact threat to the Earth. ASAS-SN consists of 24 individual 14 cm telescopes, distributed around the globe with six units located at the Hawaii station of the Las Cumbres Observatory, South Africa, Texas, China and two at Chile. ASAS-SN currently works in the optical wavelength range and is survey to monitor daily the entire night sky. The  $V$ -band used in ASAS-SN is Johnson  $V$ -band filter. In addition, ASAS-SN is now focusing on fainter objects in the  $g$ -band and the rate of data collection has been improved to 20 h, which will make ASAS-SN discover more variable objects in greater detail than before. Due to

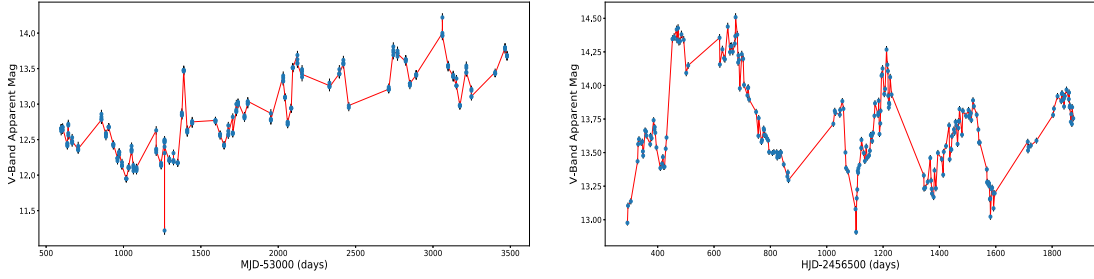


**Figure 1.** Light curves of PKS 2155-304 in the V-band from CSS (left panel) and in the V-band from ASAS-SN (right panel).

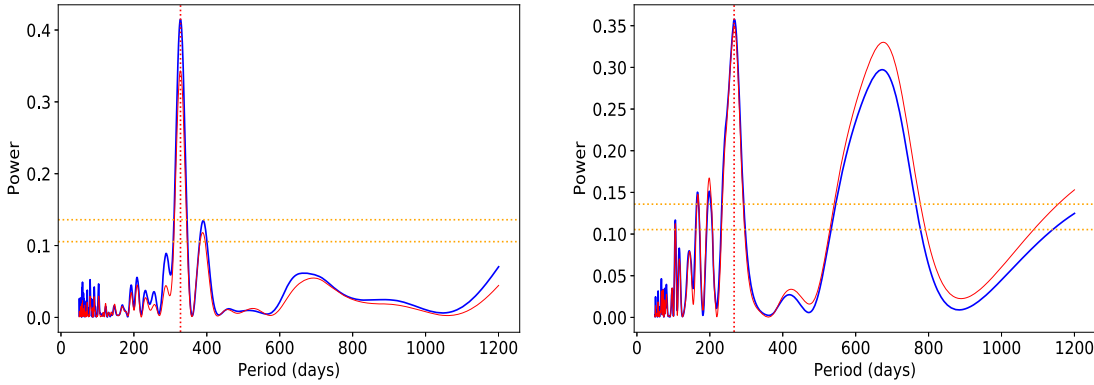


**Figure 2.** The powers determined through the GLSP method applied to the CSS light curve (left panel) and to the ASAS-SN light curve (right panel). The solid blue line in each panel represents the GLSP power of CSS and ASAS-SN light curves, and the solid red line represents the GLSP power of the evenly sampled CSS and ASAS-SN light curves. The vertical red dotted line in each panel marks the position of the corresponding peak of the power. The orange dotted lines represent significance level at 99.99% and 99.9999%, respectively.

unknown magnitude difference between ASAS-SN V-band and g-band light curves in PKS 2155-304, and due to quite short time duration of the ASAS-SN g-band light curve, the ASAS-SN g-band light curve is not taken into account in this paper.

PKS 2155-304 has been observed for many years and has shown optical QPOs. In order to test the optical QPOs in the CSS and ASAS-SN light curves, the following commonly accepted methods are applied: the generalized Lomb-Scargle periodogram (GLSP) method (Bretthorst 2001; VanderPlas 2018), the weighted wavelet Z-transform (WWZ) technique (An et al. 2013), the epoch-folded method and the redfit method (Schulz & Mudelsee 2002).

Differing from the Lomb-Scargle algorithm (Lomb 1976; Scargle 1982), the GLSP method (Zechmeister & Kürster 2009) not only considers the errors associated with the fluxes, but also uses sinusoids plus constant rather than sinusoidal functions as a fitting function. As well discussed in Zechmeister & Kürster (2009), let  $y(t) = a \cos \omega t + b \sin \omega t + c$  be the fitting function and  $y_i$  be the  $N$  measurements of a time series at time  $t_i$  with errors  $\sigma_i$ . Then at given frequency  $\omega$ , let the squared difference

between  $y(t)$  and  $y_i$  be minimized:

$$\chi^2 = \sum_{i=1}^N \frac{[y_i - y(t_i)]^2}{\sigma_i^2}. \quad (1)$$

Furthermore, the power  $P(\omega)$  normalized to unity by  $\chi_0^2$  ( $\chi^2$  for the weighted mean) can be written as:

$$P(\omega) = \frac{\chi_0^2 - \chi^2(\omega)}{\chi_0^2} \quad (2)$$

Figure 2 shows the powers from the GLSP method. Through the CSS light curve, there is a clear peak around  $328 \pm 4$  days with significance level higher than 99.9999% (false alert probability 0.000001 in GLSP). As discussed in VanderPlas (2018), the significance is usually expressed in terms of a false alarm probability, encoding the probability of measuring a peak of a given height (or higher) conditioned on the assumption that the data consists of Gaussian noise with no periodic component. Through the ASAS-SN light curve, there is a clear peak around  $267 \pm 8$  days with significance level higher than 99.9999% (false alert probability 0.000001 in GLSP). Meanwhile, there is an additional peak of  $689 \pm 14$  days in

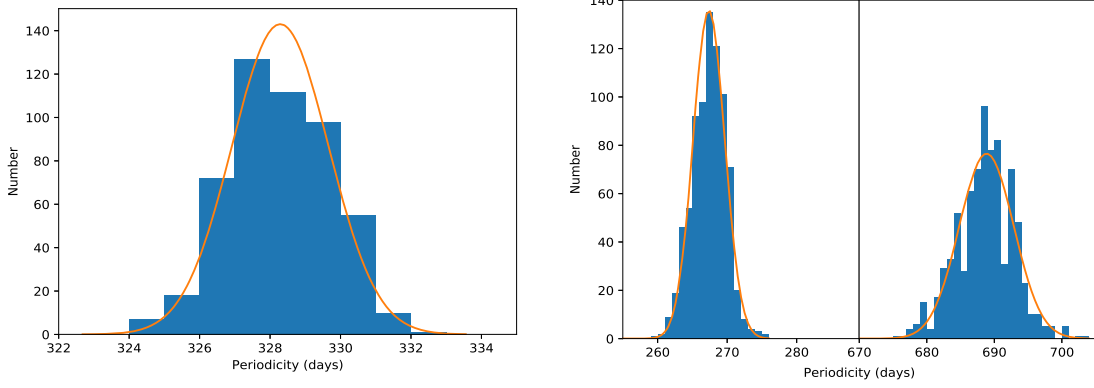


**Figure 3.** The left panel displays bootstrap method determined distribution of the periodicity about  $328 \pm 4$  days from CSS and the right panel shows bootstrap method determined distributions of the periodicity about  $267 \pm 8$  days and the second periodicity about  $689 \pm 14$  days from ASAS-SN. The solid orange line in each panel marks the best Gaussian Fitting of periodicity distribution.

ASAS-SN light curve. The uncertainties of the periodicities are determined by the widely applied bootstrap method leading to periodicity distribution shown in Figure 3. Meanwhile, based on the GLSP power properties shown in Figure 2, quality of 300 days QPOs as discussed in Gierlinski et al. (2008) can be estimated by  $T/\delta T \sim 11.3$  ( $T$  as periodicity and  $\delta T$  as full width at half maximum) in CSS light curve and 5.2 in ASAS-SN light curve, indicating there is a high quality periodicity.

In addition, based on Figure 1, the variability amplitude in the CSS light curve (standard deviation about 0.54) is about 1.6 times larger than the variability amplitude in the ASAS-SN light curve (standard deviation about 0.34). The definite reason of the different variability amplitudes (probably due to intrinsic variability related to central accreting process) is unknown. But the quite different variability amplitudes have apparent effects on detecting QPOs through GLSP, probably leading to different peak values in the GLSP power. So the data of CSS and ASAS-SN are not put together.

WWZ first proposed by Foster (1996) can be well applied to estimate and determine QPOs (Torrence & Compo 1998; An et al. 2013; Li et al. 2021), especially in unevenly sampled time series, based on three trial functions:  $1(t)$ ,  $\cos[\omega(t - \tau)]$  and  $\sin[\omega(t - \tau)]$ . The  $1(t)$  represents a constant function, since the function first described by Foster (1996).  $w_\alpha = \exp(-c\omega^2(t_\alpha - \tau)^2)$  ( $\alpha = 1, 2, 3$ ) is the statistical weight and in which  $c$  is a tunable parameter. The WWZ power is defined with

$$\text{WWZ} = \frac{(N_{\text{eff}} - 3)V_y}{2(V_x - V_y)}. \quad (3)$$

$N_{\text{eff}}$  represents the effective number density of data points, and the weighted variations of data  $x$  and model function  $y$  are  $V_x$

and  $V_y$ , respectively. These factors are described as:

$$N_{\text{eff}} = \frac{(\sum w_\alpha)^2}{\sum w_\alpha^2} = \frac{[\sum e^{-c\omega^2(t_\alpha - \tau)^2}]^2}{\sum e^{-2c\omega^2(t_\alpha - \tau)^2}}, \quad (4)$$

$$V_x = \frac{\sum_\alpha w_\alpha x^2(t_\alpha)}{\sum_\lambda w_\lambda} - \left[ \frac{\sum_\alpha w_\alpha x(t_\alpha)}{\sum_\lambda w_\lambda} \right]^2 = \langle x|x \rangle - \langle 1|x \rangle^2, \quad (5)$$

$$V_y = \frac{\sum_\alpha w_\alpha y^2(t_\alpha)}{\sum_\lambda w_\lambda} - \left[ \frac{\sum_\alpha w_\alpha y(t_\alpha)}{\sum_\lambda w_\lambda} \right]^2 = \langle y|y \rangle - \langle 1|y \rangle^2. \quad (6)$$

In Figure 4, the powers show clear peaks at  $\sim 328$  days in the CSS light curve and at  $\sim 266$  days in the ASAS-SN light curve, respectively. The periodicities determined through the WWZ technique are well consistent with the results determined by the GLSP method.

Through the CSS light curve, both GLSP and WWZ show a clear peak at about 328 days. Meanwhile, through the ASAS-SN light curve, besides the peak about 267 days, there is an additional second peak around 689 days through the GLSP method. In order to confirm the periodicity around 300 days, the epoch-folded method is applied. The left panel of Figure 5 shows the folded CSS light curve with periodicity about 328 days and with zero-point corresponding to MJD = 53597.542. The right panel of Figure 5 shows the folded ASAS-SN light curve with periodicity about 267 days and with phase zero-point corresponding to HJD = 2456752.777. The epoch-folded light curves can be well described by sinusoidal function shown as solid purple lines in Figure 5, to support the periodicity around 300 days. In order to test the second periodicity around 689 days detected in the ASAS-SN light curve by the GLSP method, two model functions are applied to

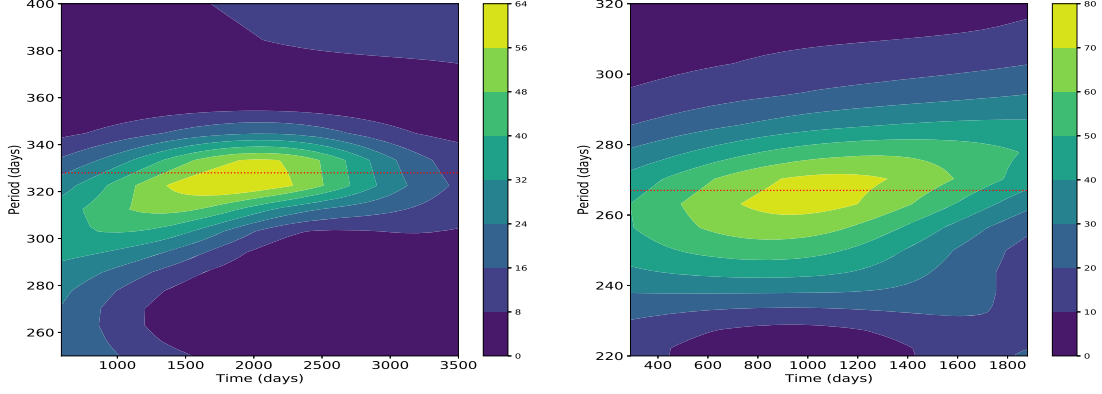


**Figure 4.** Power properties through WWZ applied to the optical CSS V-band light curve (left panel) and to the optical ASAS-SN V-band light curve (right panel). The horizontal dotted red line in each panel marks the position of the corresponding periodicity.

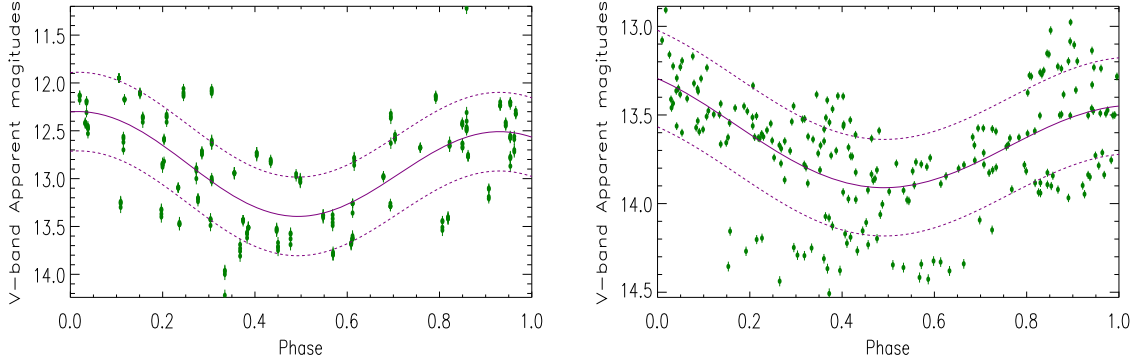


**Figure 5.** The epoch-folded CSS light curve with a 328 day periodicity (left panel) and the epoch-folded ASAS-SN light curve with periodicity of about 267 days (right panel). The solid purple lines are the best-fitting descriptions by sinusoidal function, and the dashed purple lines show the corresponding 1RMS scatters.

describe the ASAS-SN light curve. The first model function (model 1) is  $a + b \times t + c \times \sin(2\pi \times t/T + \phi_0)$  with periodicity  $T$  as a free model parameter, leading to the best descriptions shown as the solid blue line in Figure 6 with  $\chi_1^2/dof_1 \sim 26\,995.2/221$  (sum of squared residuals divided by degree of freedom) with determined  $T \sim 267$  days totally similar as the GLSP determined first periodicity. The second model function (model 2) is  $a + b \times t + c \times \sin(2\pi \times t/689 + \phi_0)$  with periodicity  $T = 689$  days (the second periodicity of 689 days detected by GLSP) as a fixed model parameter, leading to the best descriptions shown as the solid green line in Figure 6 with  $\chi_2^2/dof_2 \sim 29\,283.1/222$ . Due to high accuracy of ASAS-SN data point, there are large  $\chi^2$  value. In addition, it is useful to determine whether periodicity of 689 days is preferred through the F-test technique. Based on the different  $\chi^2/dof$  values for Model 1 and Model 2, the calculated  $F_p$  value is about

$$F_p = \frac{\frac{\chi_2^2 - \chi_1^2}{dof_2 - dof_1}}{\chi_1^2/dof_1} \sim 18.7. \quad (7)$$

Based on  $dof_2 - dof_1$  and  $dof_1$  as number of dofs of the F distribution numerator and denominator, the expected value from the statistical F-test with confidence level about 0.0021% will be near to  $F_p$ . Therefore, the confidence level is higher than 99.9979% (1%–0.0021%), higher than  $3\sigma$ , to support that periodicity of 267 days is preferred, rather than the periodicity of 689 days. Therefore, there are no further discussions on the periodicity of 689 days.

A simple fact is that we discover the  $T \sim 328$  days periodicity from data of the CSS light curve and the  $T \sim 267$  days periodicity from data of ASAS-SN. The results are similar to the optical QPOs with a periodicity of 317 days in the R-band in Zhang et al. (2014), a periodicity of 315 days in VRIJHK bands in Sandrinelli et al. (2014) and a periodicity of 315 days in R-band in Sandrinelli et al. (2018), strongly supporting the expected optical QPOs with periodicity about 300 days in the well-known blazar PKS 2155-304.

However, the presence of red noise at the optical band can affect the detected QPOs in AGN. It not only can bury possible QPOs signal, but also may spuriously mimic few-cycle sinusoid-

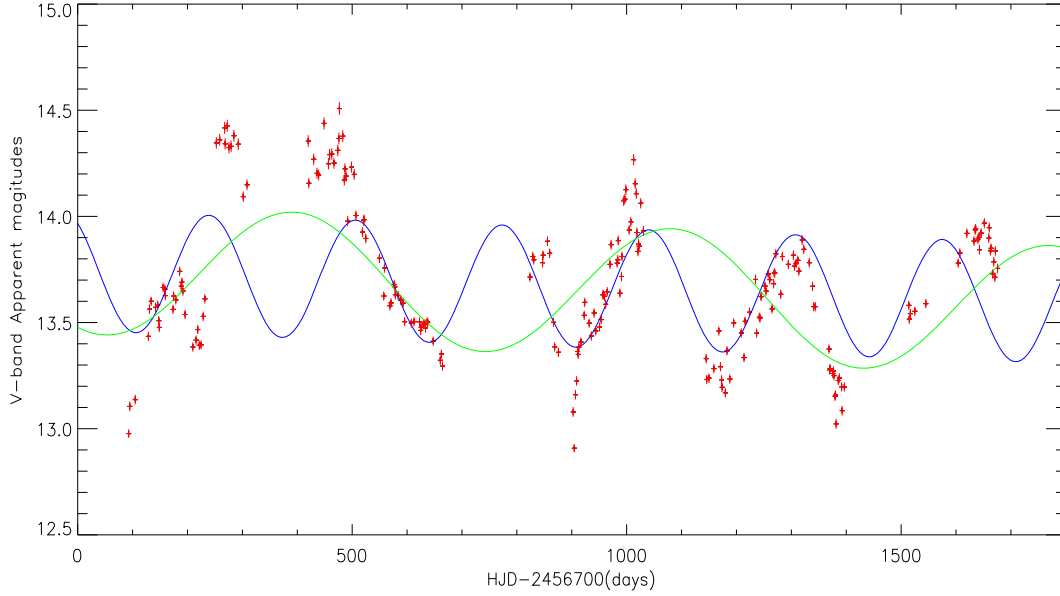


**Figure 6.** Light curve (red plus) of PKS 2155-304 in the V-band from ASAS-SN. The solid blue line shows the best fitting result with periodicity as a free model parameter, the solid green line represents the best fitting result with fixed periodicity.

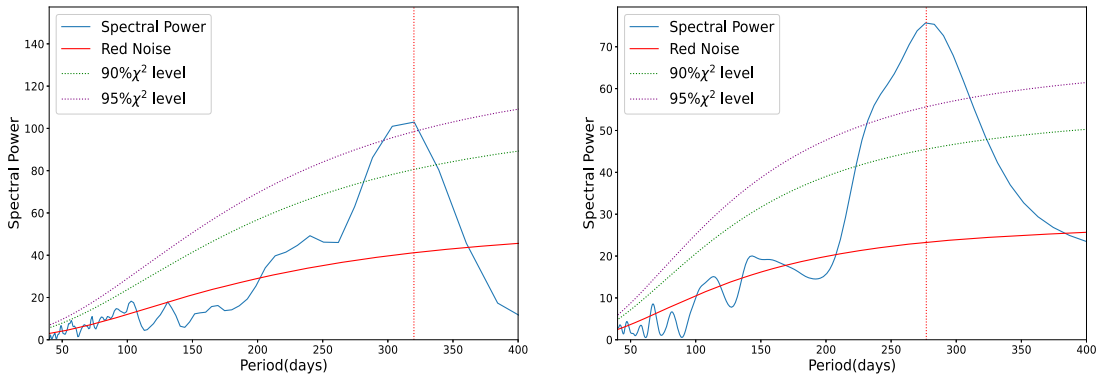


**Figure 7.** The power spectrum calculated by the redfit method applied to the CSS light curve (left panel) and the ASAS-SN (right panel) light curve.

like periods (Krishnan et al. 2021). Covino et al. (2019) has shown that some periodicities reported in AGNs appear poorly justified, but Ren et al. (2021) argued that red noise can hardly be responsible for long-term QPOs. In the paper, the influence of red noise is eliminated. Schulz & Mudelsee (2002) provided a computer program (redfit) which can estimate red-noise spectra from unevenly spaced data and give the confidence level. In addition, this program is based on two assumptions (Xiong et al. 2017): (1) the noise background can be approximated by continuous autoregressive (CAR); (2) the distribution of data points is not too clustered. Based on the redfit method, the influence of red noise in PKS 2155-304 in CSS and ASAS-SN light curves is checked in Figure 7. It is obvious that the determined periodicities are around 320 days and 277 days through the redfit method applied to CSS and ASAS-SN light

curves, respectively, similar as the results by GLSP, WWZ and epoch-folded method. What is more, the confidence levels of the periodicity in CSS and ASAS-SN light curves are both much higher than 95%.

Moreover, the damped random walk (DRW) process and/or continuous autoregressive (CAR) are used to examine the probability of detecting fake QPOs. The CAR process is discussed in Kelly et al. (2009):

$$dX(t) = -\frac{1}{\tau}X(t) + \sigma\sqrt{dt}\epsilon(t) + bdt, \quad \tau, \sigma, t > 0, \quad (8)$$

where  $\tau$  and  $\sigma$  are intrinsic characteristic variability amplitude and timescale, respectively.  $\epsilon(t)$  is a white noise process, and  $X(t)$  is the AGN light curve and  $\tau\sigma^2/2$  is the variance. According to the public code JAVELIN (Just Another Vehicle

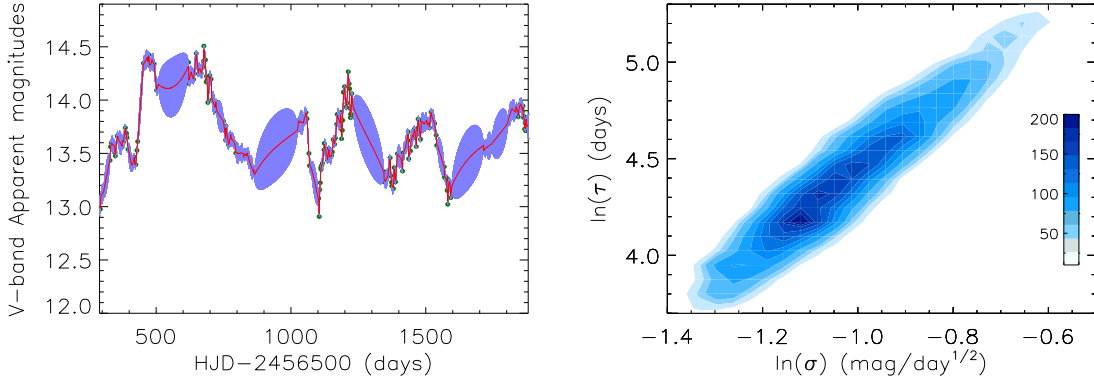


**Figure 8.** The DRW-determined best descriptions to the light curve of PKS 2155-304 (left panel) and the posterior distributions of  $\tau$  and  $\sigma$  (right panel). The solid red line represents the best descriptions and areas filled with light blue show the corresponding  $1\sigma$  confidence bands and solid green dots are the data of PKS 2155-304 from ASAS-SN in the left panel.

for Estimating Lags In Nuclei) (Kozłowski et al. 2010; Zu et al. 2013), the  $\tau$  of light curve in CSS and ASAS-SN is  $132 \pm 55$  days and  $83 \pm 36$  days, respectively. Here, due to higher quality of ASAS-SN light curve, only the best descriptions to ASAS-SN light curve is shown in the left panel of Figure 8. Moreover, the effects of insufficient data sampling can be simply discussed. Based on the best descriptions, an evenly sampled light curve (time step about 0.8 day) can be determined and shown as the solid red line in the left panel of Figure 8. Then, the solid red line in the right panel of Figure 2 shows the GLSP power properties determined from the evenly sampled ASAS-SN light curve, similar as the GLSP power properties from the observed ASAS-SN light curve. Similar results can be found in the left panel of Figure 2 to the observed CSS light curve and the evenly sampled CSS light curve (time step about 0.2 day). So that, the insufficient data sampling has few effects on our final results.

The posterior distributions of  $\tau$  and  $\sigma$  determined by Markov Chain Monte Carlo (MCMC) (Foreman-Mackey et al. 2013) technique are presented in the right panel of Figure 8. Then it is interesting to determine whether fake QPOs can be detected in CAR process created light curves. Based on Equation (8), the 1000 artificial light curves are created by the following four steps. First, the CAR process parameters are accepted as  $\tau = 132$  days (83 days),  $\tau\sigma^2/2 = 0.29$  (0.29 as the variance of the CSS light curve) ( $\tau\sigma^2/2 = 0.11$  with 0.11 as the variance of the ASAS-SN light curve) and  $bdt = 12.87$  (12.87 as the mean value of the CSS light curve) ( $bdt = 13.69$  with 13.69 as the mean value of the ASAS-SN light curve). Second, time information  $t$  is the same as that of the CSS (ASAS-SN) light curve. Third, the white noise  $\epsilon(t)$  here is randomly created with *randomn* function in IDL. Fourth, after 1000 loops, 1000 artificial light curves can be created by CAR process. Then fake QPOs are detected among the artificial light curves based on the following three criteria. First, the light curve can show well

QPOs with GLSP determined peak value higher than 0.3 (peak values in Figure 2 higher than 0.35); Second, the periodicity of the light curve is between 100 and 500 days; Third, the light curve can be well fit with epoch-folded method. Among the CAR process simulated 1000 light curves with  $\tau$  and  $\sigma$  determined from the CSS light curve (ASAS-SN), there are four light curves (eight light curves) with determined QPOs based on the three criteria above. The probability of detecting fake QPOs is 0.4% in CSS and 0.8% in ASAS-SN light curve. In addition, a CAR process created light curve with fake QPOs is shown as an example in the left panel of Figure 9, and the corresponding epoch-folded light curve shown in the right panel of Figure 9 with best fitting results by sinusoidal function.

### 3. Discussions

There are several theoretical models which can be applied to explain the optical QPOs in PKS 2155-304. In this paper, the relativistic frame-dragging effect, the binary black hole model and the jet precession model are mainly discussed as follows.

Relativistic frame-dragging effect has been primordially applied to describe the QPOs in galactic X-ray binaries with central spinning black holes (Cui et al. 1998; Stella & Vietri 1998; Ingram & Motta 2019). It is a general relativistic effect related to central accretion discs (Fukumura et al. 2009; Ingram & Motta 2019; Zhang 2021), and it can be also applied in blazars (Marscher et al. 2008; Liu et al. 2021). As more recent discussions in Bhatta (2021), “the rapidly spinning supermassive black hole can warp spacetime and give rise to the precession of the disk owing to the Lense-Thirring precession.” The Lense-Thirring precession frequency (Cui et al. 1998) is given by

$$\nu_{\text{LT}} = 6.45 \times 10^4 |a_*| \left( \frac{M}{M_\odot} \right)^{-1} \left( \frac{r}{r_g} \right)^{-3} \text{ Hz.} \quad (9)$$

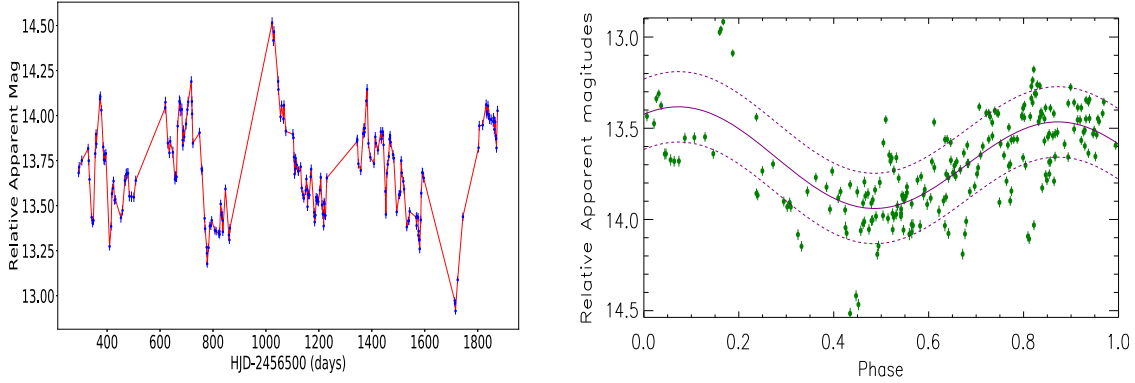


**Figure 9.** An example of light curve with fake QPOs by CAR process (left panel) and corresponding epoch-folded light curve with periodicity about 400 days (right panel). The solid purple line represents the best-fitting descriptions by sinusoidal function, and the dashed purple lines show the corresponding 1RMS scatters in the right panel.

In this equation,  $a_*$  is an angular momentum parameter.  $M$  represents the mass of black hole, and  $r$  is the radii of emission regions and  $r_g = GM/c^2$  is the Schwarzschild radii. Moreover, Gierlinski et al. (2008) reported that RE J1034+396 has an X-ray periodicity of 1 h. Meanwhile, the central BH mass of RE J1034+396 reported in Czerny et al. (2016); Jin et al. (2020) is about  $5 \times 10^6 M_\odot$ . RE J1034+396 is chosen as a standard case with the Lense-Thirring precession determined X-ray QPOs from the direct vicinity (about 10 Schwarzschild radii) of the black hole as discussed in Gierlinski et al. (2008). Meanwhile, if simply accepted that the optical QPOs of PKS2155-304 are also related to the Lense-Thirring precession, the central BH mass of PKS 2155-304 can be estimated, assumed optical emission regions are about 100 ~ 200 Schwarzschild radii.

The central BH mass of PKS 2155-304 with optical periodicity about 300 days would be  $4.5 \times 10^6 M_\odot \sim 3.6 \times 10^7 M_\odot$  with

$$M_{\text{BH}} \sim \frac{300 \text{ days}}{1 \text{ hr}} \times 5 \times 10^6 M_\odot \left( \frac{r_{\text{opt}}}{10} \right)^{-3}. \quad (10)$$

The mean mass can be roughly estimated as  $1.5 \times 10^7 M_\odot$ , which is similar as the BH mass in PKS 2155-304 reported in Lachowicz et al. (2009) through X-ray QPOs properties. However, the estimated BH mass is quite smaller than  $10^9 M_\odot$  determined by host galaxy absolute magnitude of PKS 2155-304 as discussed in Falomo et al. (1991), Kotilainen et al. (1998), Sandrinelli et al. (2014), which is about two magnitudes higher than our estimated BH mass, probably due to the following two reasons. On one hand, according to Kormendy & Ho (2013), the relation between black hole mass and magnitude has large intrinsic scatter about 0.31. On the other hand, the beaming effects would affect the host galaxy absolute magnitude, considering that a simple PSF function should be not efficient enough to totally describe central

emissions including beaming effects. If there were independent methods applied to determine the central BH mass of PKS 2155-304, it would provide further clues to support whether the relativistic Frame-dragging effect is preferred in PKS 2155-304.

Besides the relativistic frame-dragging effect, the binary black hole (BBH) model can be applied to explain the optical QPOs in PKS 2155-304, as the reported long-term optical QPOs in Britzen et al. (2020), Yang et al. (2021), Liao et al. (2021), and O’Neill et al. (2022). Under the framework of the BBH model, the space separation  $A_{\text{BBH}}$  of the central binary black hole should be

$$A_{\text{BBH}} = 0.432 \times M_8 \times \left( \frac{P_{\text{BBH}}/\gamma T}{2652 M_8} \right)^{\frac{2}{3}}, \quad (11)$$

where  $M_8$  is the central total BH mass in units of  $10^8 M_\odot$  and  $P_{\text{BBH}}$  is the QPOs periodicity. If  $M_{\text{BH}} \sim 10^9 M_\odot$ , determined by the absolute magnitude of host galaxy of PKS 2155-304, is accepted as the total BH mass, the expected space separation is about

$$A_{\text{BBH}} \sim 0.004 \text{ pc} \sim 4.8 \text{ light - days}. \quad (12)$$

So small space separation indicates that it is hard to spatially resolve central binary black hole in central regions of PKS 2155-304 in the near future. However, so small space separation in the BBH model is also reported in literature, such as Li et al. (2021) used the BBH model to explain QPOs with periodicity of 850 days in OT 081, with estimated space separation about 0.0076 pc.

Jet precession (Caproni et al. 2013; Mangalam 2018; Ren et al. 2021) is also a possible explanation for the QPOs shown in the long-term light curves. It assumes helical structure in a relativistic jet (Bhatta 2018; Zhang et al. 2021). Brightness of source varies with the viewing angle (Zhang et al. 2014; Li et al. 2017). This model has been successfully used to other

AGNs. Bhatta et al. (2016) reported that OJ 287 has a periodicity of 400 days. Caproni et al. (2017) reported that PG 1553+113 has a periodicity of 2.24 yr at 15 GHz from data of the MOJAVE/2 cm Survey Data Archive (during 2009–2016). Sarkar et al. (2021) reported that 3C 454.3 shows a periodicity of 47 days in  $\gamma$ -ray and optical bands. Tripathi et al. (2021) reported that AO 0235+164 has a periodicity of 965 days with the radio band data from the University of Michigan Radio Astronomical Observatory during 1980–2012. Zhang & Wang (2021) reported that J0849+5108 shows a periodicity of 176 days at the 15 GHz from observations by the Owens Valley Radio Observatory. It is interesting to consider jet precession model in PKS 2155-304.

There are the 0.7 day periodicity in the ultraviolet band (Urry et al. 1993) and 4.6 h periodicity in the X-ray band (Lachowicz et al. 2009), which are quite different from 300 days optical periodicity of PKS 2155-304 shown in our paper. Considering the differences of the observation time and the radiation area between optical band and other bands, it is possible to detect different QPOs in different bands. Therefore, more efforts should be necessary to check the jet precession model to explain the QPOs in PKS 2155-304.

#### 4. Summaries and Conclusions

The main summaries and conclusions are as follows.

1. Through the CSS and ASAS-SN light curves, optical QPOs with periodicity about 300 days are reported in PKS 2155-304, which are well consistent with previously reported optical QPOs in the literature through light curves in different optical bands and from different projects, providing strong evidence to support the optical QPOs with periodicity about 300 days in PKS 2155-304.
2. The QPOs in the CSS light curve have about 8.8 cycles and in the ASAS-SN light curves have about 6 cycles.
3. If the relativistic frame-dragging effect is applied to explain the optical QPOs in PKS 2155-304, the estimated central BH mass should be about  $10^7 M_{\odot}$ , which is quite smaller than that estimated by absolute magnitude of host galaxy of PKS 2155-304.
4. If the BBH model is applied to explain the optical QPOs, the total BH mass estimated by absolute magnitude of host galaxy would lead the central space separation about 0.004 pc between the central two black holes.
5. The optical 300 days QPOs are different from that in ultraviolet and X-ray bands found in previous references. If the jet precession model is applied, different bands may have similar QPOs. However, it is possible to detect different QPOs in different bands due to different observation time and radiation area.

#### Acknowledgments

We gratefully acknowledge our referee for reading our paper again carefully and patiently, and re-giving us constructive comments and suggestions to greatly improve the paper. This work is supported by the National Natural Science Foundation of China (Grant Nos. 11873032 and 12173020). This paper has made use of the data from the CSS and ASAS-SN projects developed rapidly moving Near Earth Objects. The CSS website is (<http://nesssi.cacr.caltech.edu/DataRelease/>). The paper has made use of the data from the ASAS-SN (<https://asas-sn.osu.edu/>). The website of JAVELIN code is (<https://github.com/nye17/javelin/>).

#### References

- Abdo, A. A., Ackermann, M., Ajello, M., et al. 2010, *ApJ*, 710, 810  
 Agarwal, A., Cellone, S. A., Andruchow, I., et al. 2019, *MNRAS*, 488, 4093  
 Aharonian, F., Akhperjanian, A. G., Anton, G., et al. 2009, *ApJ*, 696, 150  
 Aharonian, F., Akhperjanian, A. G., Aye, K. M., et al. 2005, *A&A*, 430, 865  
 An, T., Baan, W. A., Wang, J. Y., et al. 2013, *MNRAS*, 434, 3487  
 Arbet-Engels, A., Baack, D., Balbo, M., et al. 2021, *A&A*, 655, 93  
 Bhatta, G. 2018, *Galax*, 6, 136  
 Bhatta, G. 2021, *ApJ*, 923, 7  
 Bhatta, G., & Dhital, N. 2020, *ApJ*, 891, 120  
 Bhatta, G., Zola, S., Stawarz, Ł., et al. 2016, *ApJ*, 832, 47  
 Bretthorst, G. L. 2001, *AIPC*, 568, 241  
 Britzen, S., Fendt, C., Witzel, G., et al. 2020, *IAUS*, 342, 250  
 Caproni, A., Abraham, Z., & Monteiro, H. 2013, *MNRAS*, 428, 280  
 Caproni, A., Abraham, Z., Motter, J. C., et al. 2017, *ApJ*, 851, 39  
 Carini, M. T., & Miller, H. R. 1992, *ApJ*, 385, 146  
 Chadwick, P. M., Lyons, K., McComb, T. J. L., et al. 1999, *ApJ*, 513, 161  
 Chevalier, J., Sanchez, D. A., Serpico, P. D., et al. 2019, *MNRAS*, 484, 749  
 Covino, S., Sandrinelli, A., & Treves, A. 2019, *MNRAS*, 482, 1270  
 Cui, W., Zhang, S. N., & Chen, W. 1998, *ApJ*, 492, 53  
 Czerny, B., You, B., Kurcz, A., et al. 2016, *A&A*, 594, A102  
 Dominici, T. P., Abraham, Z., & Galo, A. L. 2006, *A&A*, 460, 665  
 Dominici, T. P., Abraham, Z., Teixeira, R., et al. 2004, *AJ*, 128, 47  
 Drake, A. J., Djorgovski, S. G., Mahabal, A., et al. 2009, *ApJ*, 696, 870  
 Edelson, R., Krolik, J., Madejski, G., et al. 1995, *ApJ*, 438, 120  
 Falomo, R., Giraud, E., Maraschi, L., et al. 1991, *ApJ*, 380, 67  
 Fan, J. H., & Lin, R. G. 2000, *A&A*, 355, 880  
 Fan, J. H., Xie, G. Z., Pecontal, E., et al. 1998, *ApJ*, 507, 173  
 Foreman-Mackey, D., Hogg, D. W., Lang, D., et al. 2013, *PASP*, 125, 306  
 Foschini, L., Ghisellini, G., Tavecchio, F., et al. 2007, *ApJ*, 657, 81  
 Foster, G. 1996, *AJ*, 112, 1709  
 Fukumura, K., Kazanas, D., & Stephenson, G. 2009, *ApJ*, 695, 1199  
 Gaur, H., Gupta, A. C., Lachowicz, P., et al. 2010, *ApJ*, 718, 279  
 Giannios, D., Uzdensky, D. A., & Begelman, M. C. 2009, *MNRAS*, 395, 29  
 Gierlinski, M., Middleton, M., Ward, M., & Done, C. 2008, *Natur*, 455, 369  
 Gupta, A. C., Banerjee, D. P. K., Ashok, N. M., et al. 2004, *A&A*, 422, 505  
 Hayasaki, K., Saito, H., & Mineshige, S. 2013, *PASJ*, 65, 86  
 Heidt, J., Wagner, S. J., & Wilhelm-Erkens, U. 1997, *A&A*, 325, 27  
 Hong, S. W., Xiong, D. R., & Bai, J. M. 2018, *AJ*, 155, 31  
 Ingram, A. R., & Motta, S. E. 2019, *NewAR*, 85, 01524  
 Jin, C., Done, C., & Ward, M. 2020, *MNRAS*, 495, 3538  
 Joshi, J. C., & Razaque, S. 2021, *MNRAS*, 505, 1718  
 Kalita, N., Gupta, A. C., & Gu, M. F. 2021, *ApJS*, 257, 41  
 Kastendieck, M. A., Ashley, M. C. B., & Horns, D. 2011, *A&A*, 531, 123  
 Katarzyński, K., Lenain, J. P., Zech, A., et al. 2008, *MNRAS*, 390, 371  
 Kelly, B. C., Bechtold, J., & Siemiginowska, A. 2009, *ApJ*, 698, 895  
 Kochanek, C. S., Shappee, B. J., Stanek, K. Z., et al. 2017, *PASP*, 129, 4502  
 Kormendy, J., & Ho, L. C. 2013, *ARA&A*, 51, 511  
 Kotilainen, J. K., Falomo, R., & Scarpa, R. 1998, *A&A*, 336, 479  
 Kozłowski, S., Kochanek, C. S., Udalski, A., et al. 2010, *ApJ*, 708, 927

- Krishnan, S., Markowitz, A. G., Schwarzenberg-Czerny, A., et al. 2021, *MNRAS*, 508, 3975
- Lachowicz, P., Gupta, A. C., Gaur, H., et al. 2009, *A&A*, 506, 17
- Li, X. P., Cai, Y., Yang, H. T., et al. 2021, *MNRAS*, 506, 1540
- Li, X. P., Luo, Y. H., Yang, H. Y., et al. 2017, *ApJ*, 847, 8
- Li, X. P., Yang, H. Y., Luo, Y. H., et al. 2018, *MNRAS*, 479, 4073
- Li, X. P., Zhao, L., Yan, Y., et al. 2021, *JApA*, 42, 92
- Liao, W. T., Chen, Y. C., Liu, X., et al. 2021, *MNRAS*, 500, 4025
- Liu, X. L., Yuan, Y. H., & Huang, H. R. 2021, *RAA*, 21, 102
- Lomb, N. R. 1976, *Ap&SS*, 39, 447
- Mangalam, A. 2018, *JApA*, 39, 68
- Marscher, A. P., Jorstad, S. G., D’Arcangelo, F. D., et al. 2008, *Natur*, 452, 966
- Miller, H. R., & McAlister, H. A. 1983, *ApJ*, 272, 26
- O’Neill, S., Kiehlmann, S., Readhead, A. C. S., et al. 2022, *ApJ*, 926, 35
- Paltani, S., Courvoisier, T. J. L., Blecha, A., et al. 1997, *A&A*, 327, 539
- Pandey, A., Gupta, A. C., Kurtanidze, S. O., et al. 2020, *ApJ*, 890, 72
- Pekeur, N. W., Taylor, A. R., Potter, S. B., et al. 2016, *MNRAS*, 462, 80
- Peñil, P., Domínguez, A., Buson, S., et al. 2020, *ApJ*, 896, 134
- Pesce, J. E., Urry, C. M., Maraschi, L., et al. 1997, *ApJ*, 486, 770
- Prokhorov, D. A., & Moraghan, A. 2017, *MNRAS*, 471, 3036
- Ren, G. W., Ding, N., Zhang, X., et al. 2021, *MNRAS*, 506, 3791
- Ren, G. W., Zhang, H. J., Zhang, X., et al. 2021, *RAA*, 21, 75
- Rieger, F. M., & Volpe, F. 2010, *A&A*, 520, 23
- Sandrinelli, A., Covino, S., & Treves, A. 2014, *ApJ*, 793, 1
- Sandrinelli, A., Covino, S., Treves, A., et al. 2018, *A&A*, 615, 118
- Sarkar, A., Gupta, A. C., Chitnis, V. R., et al. 2021, *MNRAS*, 501, 50
- Scargle, J. D. 1982, *ApJ*, 263, 835
- Schulz, M., & Mudelsee, M. 2002, *CG*, 28, 421
- Schwartz, D. A., Doxsey, R. E., Griffiths, R. E., et al. 1979, *ApJ*, 229, 53
- Shappee, B. J., Prieto, J. L., Grupe, D., et al. 2014, *ApJ*, 788, 48
- Shimmins, A. J., & Bolton, J. G. 1974, *AuJPA*, 32, 1
- Smith, K. L., Mushotzky, R. F., Boyd, P. T., et al. 2018, *ApJ*, 860, 10
- Stella, L., & Vietri, M. 1998, *ApJ*, 492, 59S
- Tarnopolski, M., Żywucka, N., Marchenko, V., et al. 2020, *ApJS*, 250, 1
- Tommasi, L., Díaz, R., Palazzi, E., et al. 2001, *ApJS*, 132, 73
- Torrence, C., & Compo, G. P. 1998, *BAMS*, 79, 61
- Tripathi, A., Gupta, A. C., Aller, M. F., et al. 2021, *MNRAS*, 501, 5997
- Urry, C. M., Maraschi, L., Edelson, R., et al. 1993, *ApJ*, 411, 614
- Valtonen, M. J., Lehto, H. J., Nilsson, K., et al. 2008, *Natur*, 452, 851
- VanderPlas, J. T. 2018, *ApJS*, 236, 16
- Wagner, S. J., & Witzel, A. 1995, *ARA&A*, 33, 163
- Xiong, D., Bai, J., Zhang, H., et al. 2017, *ApJS*, 229, 21
- Yang, J. P., Cao, G., Zhou, B., et al. 2021, *PASP*, 133, 4101
- Zechmeister, M., & Kürster, M. 2009, *A&A*, 496, 577
- Zhang, B. K., Zhao, X. Y., Wang, C. X., et al. 2014, *RAA*, 14, 933
- Zhang, H. Y., Yan, D. H., & Zhang, P. F. 2021, *ApJ*, 919, 58
- Zhang, P. F., & Wang, Z. X. 2021, *ApJ*, 914, 1
- Zhang, P. F., Yan, D. H., Liao, N. H., et al. 2017, *ApJ*, 835, 260
- Zhang, X. G. 2021, *MNRAS*, 502, 1158
- Zhang, Z. L., Gupta, A. C., Gaur, Haritma, et al. 2021, *ApJ*, 909, 103
- Zu, Y., Kochanek, C. S., Kozłowski, S., et al. 2013, *ApJ*, 765, 106
- Żywucka, N., Tarnopolski, M., Marchenko, V., et al. 2021, arXiv:2112.01761